Program Digest, 2019 IEEE International Ultrasonics Symposium (IUS)
Glasgow, Scotland, October 6-9, 2019

A Miniaturized (100 µm x 100 µm) 45 kHz Aluminum Nitride Ultrasonic Transducer for Airborne Communication and Powering

Pietro Simeoni and Gianluca Piazza
ECE Department, Carnegie Mellon University
Pittsburgh, PA, USA
pietros@andrew.cmu.edu

Abstract— **We report on the demonstration of a highly compact (100 µm x 100 µm) piezoelectric nanoscale ultrasonic transducer (pNUT) characterized by an extremely thin (≈100 nm) aluminum nitride (AlN) active layer and designed to operate in the low ultrasounds frequency range (40 kHz). We analyze the pNUT response by means of an equivalent circuit model and compare it to the measured response of the pNUT to ultrasounds excitation.**

I. Introduction

During the last few decades there has been a growing interest in Piezoelectric Micromachined Ultrasonic Transducers (pMUTs) due to their increasing number of applications in sectors like healthcare [1] and security [2]. An emerging application for ultrasound transducers consists in enabling communication and wireless power transfer between small Internet of Things (IoT) nodes. Rekhi et al. [3] make a thorough analysis on the feasibility of the method, taking advantage of the fact that ultrasounds in the frequency range below 100 kHz experience low attenuation in air (< 3dB/m). Typically the thickness of the film stack used in pMUTs ranges from 1 µm to 10 µm, which makes the footprint necessary for sub-100 kHz resonance impractical for integration with advanced electronic nodes. For a given frequency of operation, a way to reduce the transducer area is scaling down the film stack below the µm range. Jiang et al. investigated thickness scaling to improve the transmission sensitivity (nm/V) of the transducers [4]. One of the limitations of thickness scaling is an increased dependence of the device stiffness on the residual stress of the deposited films [5]. Since residual stress becomes harder to control in thinner films, we demonstrate a novel transducer geometry that departs from the traditional circular plate and aims at reducing the influence of residual stresses on the frequency of operation of the device. We dub this device the 4-beams piezoelectric nanoscale ultrasonic transducer (pNUT, Fig.1).

II. Device Principle of Operation

The demonstrated geometry consists of 4 beams connected to a central suspended plate. A 100 nm thick AlN layer is sandwiched between two platinum (Pt) layers. The geometry is patterned by generating slits in the AlN layer (Fig. 1d). These cuts allow for the residual stresses in the films to be partially relaxed, reducing their influence in defining the equivalent stiffness of the flexure and therefore minimizing the risk of tearing. It is important to notice that allowing the structure to deform will also make it bend out of plane when the residual

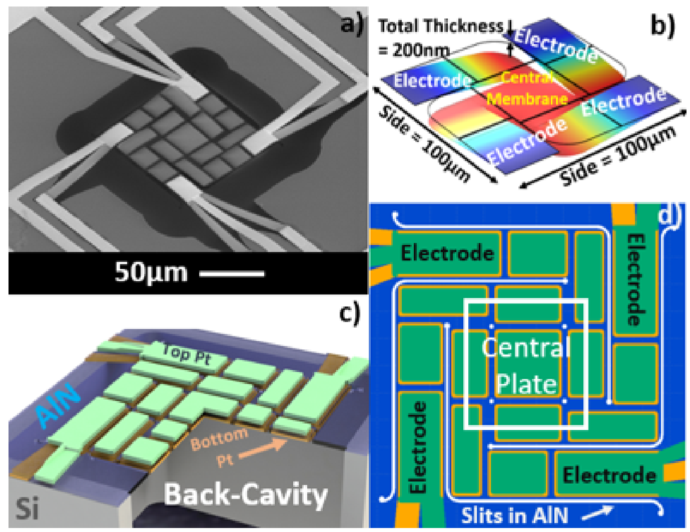

Fig. 1. a) SEM picture of the fabricated device. b) First resonance mode shape. c) 3D rendering of the pNUT. d) Transducer layout.

stresses relax upon release. In fact, the demonstrated geometry is a compromise between the traditional, fully-clamped circular plate, which is highly sensitive to residual stresses for highly scaled films, and a cantilevered structure, which is able to completely relax the residual stresses while being free to deform out of plane. The electrodes are deposited with different thicknesses, 20 nm and 80 nm, to shift the beams neutral axis away from the center of the piezoelectric layer and generate a net polarization when the beams deflect [6]. Only the metal deposited at the anchored region of the beams is used to sense the piezoelectric transduction, while the rest of the metal is left floating on the beams tips and on the central plate to increase the equivalent mass of the resonator and keep the resonance frequency in the targeted range. We segmented the Pt layers to mitigate the effect of residual stresses and out-of-plane bending of the structure. All corners in the metals and at the anchors regions are rounded to avoid stress concentration points resulting in the tearing of the thin AlN layer. Because of the small footprint of the device, it is important to account for the effect of the back-cavity volume on the transducer frequency response. As we will show in the next section this effect is especially important at low frequencies. This first demonstration is characterized by a small back-cavity to facilitate the fabrication process while proving the pNUT concept. We anticipate that future iterations of the transducer will present greater back-cavity volumes and therefore higher electrical outputs.

III. Equivalent Circuit Model

Three different physics domains are involved in the operation of the pNUT: acoustic, mechanical and electrical. In the acoustic domain pressure waves travel through air to the transducer and its back-cavity. The incident waves will set the structure in motion. The dynamics of the structure is described in the mechanical domain. Finally, the stresses and strains generated in the transducer as it deforms will be converted into voltages and currents by the direct piezoelectric effect. The electrical behavior of the device is described by the electrical domain portion of the equivalent model. In order to describe the three domains simultaneously, we use an equivalent electrical circuit, where inductors, capacitors, and resistors represent inertial, storing, and dissipative effects respectively, while transformers represent the transduction from one domain to another. We also notice that a lumped circuit model is appropriate in our case, since, at the frequency of operation, the pNUT dimensions are much smaller than the acoustic wavelength ($\lambda \approx$0.85 cm at 40 kHz). The equivalent circuit model is shown in Fig. 2.

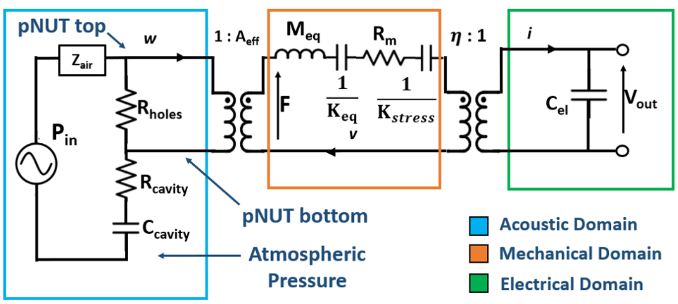

Fig. 2. pNUT equivalent circuit model.

A. Acoustic Domain

In the acoustic domain the acoustic pressure of the incident wave is represented by an AC voltage source. The source impedance is represented by the radiation impedance of air, which can be safely neglected in the model as it is much lower than the transducer impedance. The pressure differential between the top and bottom of the device is smaller than the acoustic pressure amplitude of the wave because of the presence of the back-cavity. As the pNUT moves from its equilibrium position, it compresses/rarefies the air in the back-cavity volume. Air acts as a spring element that opposes the membrane motion by reducing the pressure drop across the suspended structure. To represent this spring effect we use an equivalent capacitance that is given by (1),

$$C_{cavity} = \frac{V}{\rho_{air} c_{air}^2} \tag{1}$$

where ρ_{air} is air density, c_{air} is the speed of sound in air and V is the volume of the back-cavity [7]. R_{holes} represents the slits that define the pNUT geometry, and act as a path to pressure equalization between the top and bottom of the membrane. It is hard to obtain an analytical expression of R_{holes} due to the complex geometry of the slits and the bending caused by stress gradients. However, a first order approximation of the value of R_{holes} can be obtained through the equivalent acoustic resistance of a rectangular slit given by (2),

$$R_{holes} = \frac{12 t_{slit} \mu_{air}}{l_{slit} w_{slit}^3} \tag{2}$$

where t_{slit},w_{slit}, and l_{slit} are the thickness, width and total length of the slits respectively, and μ_{air} is air viscosity [7]. Another resistor is added in series with C_{cavity}, that we call R_{cavity}, to describe the losses due to the viscous forces inside the cavity and the friction between air and the membrane surface. Due to the complexity of the viscous interactions between air and the device surface it is hard to obtain an analytical expression of this component. In the frequency range we are operating at, typical values of R_{cavity} are expected to give quality factors ranging from 10 to 100 [8][9], and the value for the specific device under test can be obtained by fitting experimental data.

B. Mechanical Domain

The transition from acoustic to mechanical domain is depicted by a transformer with turn ratio equal to the effective area of the device, described by the equation (3)

$$A_{eff} = 4WL \int_0^1 Y(x)dx + A_{center} \tag{3}$$

where W and L are the width and length of the beams, $Y(x)$ is the beam mode shape, and A_{center} is the area of the central plate. In this model $Y(x)$ is approximated as a clamped-guided beam mode shape. The values of L_m and C_m can be obtained with expressions (4) and (5) respectively,

$$M_{eq} = \rho_{eff} t (4WL \int_0^1 Y(x)^2 dx + (L-W)^2) \tag{4}$$

$$\frac{1}{K_{eq}} = \frac{1}{4k_{cf}} = \frac{1}{4}\frac{L^3}{12EI_{eff}} \tag{5}$$

where t is the total thickness of the pNUT, ρ_{eff} is the effective density of the stack, k_{cg} is the stiffness of a clamped-guided beam and EI_{eff} is the effective flexural rigidity of the beams. R_m represents the internal losses of the structure. An additional capacitor, C_{stress} is added to represent the stiffening caused by the tensile residual stresses.

C. Electrical Domain

The transduction from mechanical to electrical domain is described by the transformer ratio η, which relates the total strain generated from the structure deflection to the electric displacement along the thickness direction through the piezoelectric coefficient $e_{31,eff}$

$$\eta = 4e_{31,eff}(z_n - z_i)WL_{el}\int_0^1 \frac{d^2Y(x)}{dx^2}dx \quad (6)$$

where z_n and z_i are the positions of the neutral axis and the center point of the piezoelectric layer along the thickness direction respectively, and L_{el} is the length of the electrodes along the beams. The output voltage is measured across the electrical capacitance C_{el} between the top and bottom electrodes,

$$C_{el} = 4\epsilon_0\epsilon_r\frac{WL_{el}}{t_{pz}} \quad (7)$$

where ϵ_0 and ϵ_r are the absolute and relative dielectric constants, and t_{pz} is the thickness of the piezoelectric layer.

IV. Fabrication Process

We show the pNUT process flow in Fig. 3. In step 1) a 20 nm Pt layer is deposited on the Si substrate and patterned by lift-off. A 100 nm AlN layer is then sputtered in an Tegal AMS sputtering system. The sputtering is carried on at low power (3 kW) to ensure the formation of smaller grains, attain good stress control and provide good c-axis orientation of the AlN film. Since photoresist spin-coated on top of the AlN films deposited at low power delaminates during the wet etching of AlN, a hard-mask approach is used to pattern the AlN layer. A 50 nm SiO_2 film is deposited on top of AlN by PECVD, and subsequently patterned in a CHF_3 RIE step. We complete step 2) in Fig. 3 by wet-etching the exposed AlN film in a CD26 developer solution. Step 3) is completed by sputtering 80 nm of Pt and patterning the top electrode with a lift-off step. Finally, the devices are released in XeF_2.

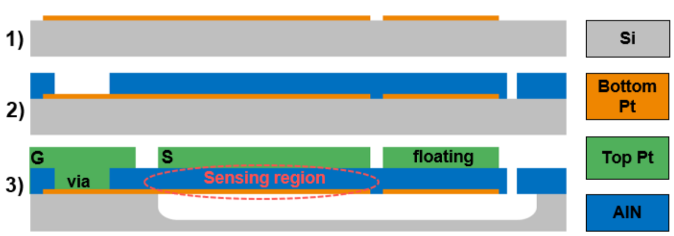

Fig. 3. 3-mask process flow used to fabricate the proposed pNUT.

The main challenge of the fabrication process is to keep the residual stress in the AlN and top Pt layers as low as possible. There are two main reasons for this: 1) the proposed geometry will only partially be able to relax the residual stress through deformations, and its equivalent stiffness will still depend on residual stress, and 2) the geometry is sensitive to stress gradients between the stacked layers that cause the structure to bend out of plane and affect the value of R_{holes}. The increased sensitivity to stress gradients is an inevitable trade-off that comes with reducing the stiffness dependence on residual stress when moving away from a fully clamped configuration.

V. Device Characterization

We extracted an electrical capacitance of 3 pF across several devices, against an expected value of 2.6 pF. We attribute the 400 fF of parassitic capacitance to the coupling between the pads through the substrate. We also measured resistances ranging from tens of Ω to several $k\Omega$ between the top and bottom electrodes of the devices. We identified the problem in the bottom Pt deposition step, where metal sputtered on the side walls of the photoresist was not completely removed during lift-off, generating a low resistance path through the AlN layer. This problem can be fixed by switching to negative photoresist for the bottom Pt lift-off and it is not an intrinsic limitation of the fabrication of devices characterized by thin AlN layers[10][11]. We represent this effect by adding a resistance, R_{par}, to the equivalent circuit model (Fig.4). Because of this issue, it was not possible to electrically characterize the motional branch of the device by direct probing in vacuum, which allows to de-embed the effects of the slits and the back-cavity volume. However, we were able to verify the device response to ultrasound with the experimental setup presented in Fig. 4. The measurement setup takes advantage of the ability of the lock-in amplifier to record low-amplitude signals buried in noise, allowing us to measure the pNUT response even with a shallow back-cavity that stiffens the mechanical response and reduces the sensitivity. Additionally, we add a trans-impedance amplifier (TIA) in the measurement loop in order to amplify the signal and ground the two electrodes so as to bypass R_{par}.

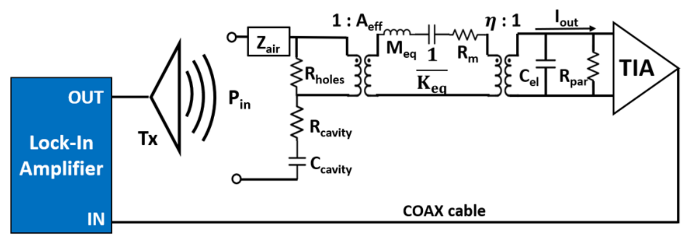

Fig. 4. Schematic of the experimental setup used to measure the pNUT frequency response to ultrasound excitation.

To excite the device we use a commercial ultrasonic transmitter with a nominal resonance frequency of 40 kHz. To perform the characterization, we first record the frequency response of the pNUT to the applied ultrasound, then we replace the device with a calibrated microphone (Type-4939 by Bruel & Kjaer), and repeat the frequency sweep to directly measure the acoustic pressure generated at the pNUT location. These two measurements give us the pressure sensitivity of the device (Fig. 5). The values of the equivalent circuit components fitting the device response are presented in TABLE I.

VI. Conclusion

We demonstrated the feasibility of a 4-beams pNUT to achieve a compact form factor while resonating at frequencies in the tens of kHz range. We measured the electrical response to ultrasound excitation by using a lock-in amplifier and a TIA. The pNUT response fits well the output of the equivalent circuit

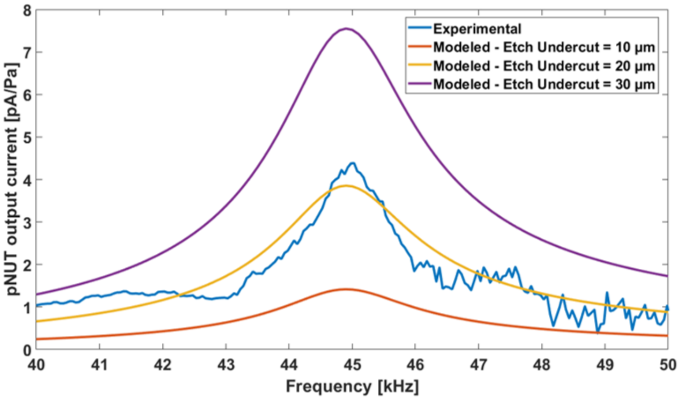

Fig. 5. Comparison between the experimental pNUT response and the output of the equivalent circuit model.

TABLE I
PARAMETERS VALUES USED TO SIMULATE THE MEASURED DEVICE

Parameter	Unit	Value	Comment
Side	μm	100	
C_{cavity}	m^5/N	1.35e-13	Volume from undercut of 20μm
R_{cavity}	N s/m^5	1.22e10	Using a quality factor of 40
R_{holes}	N s/m^5	3.77e9	
M_{eq}	kg	1.53e-11	
K_{eq}	N/m	0.32	
$1/C_{stress}$	N/m	2.8*K_{eq}	
R_m	N s/m	2.21e-9	Using a quality factor of 1000
C_{el}	F	2.6e-12	
A_{eff}	m^2	7.02e-9	
η	N/V	3.55e-8	

model. Future work includes modifying the fabrication process to replace the XeF_2 top release with a back-etch DRIE step, and increase the volume of the back-cavity while maintaining a thick substrate in the clamped region of the anchors. As the back-side cavity volume is increased we expect the output of the pNUT to increase to the nA/Pa range, comparable to its much larger counterparts. We can use the measured electrical capacitance to calculate the open-circuit receive sensitivity in mV/Pa and compare an open-cavity pNUT performance (i.e. with infinite C_{cavity}) with data from literature. We take literature data and normalize it by quality factor to compare transducers with different frequencies of operation. Then, we convert the transmit sensitivity (nm/V) into receive sensitivity (mV/Pa) by means of the following proportionality relations,

$$Tx_{Sensitivity} = \frac{d}{V} \propto \frac{F_{eq}\eta}{K_{eq}F_{eq}} \propto \frac{At}{t^3} \propto \frac{A}{t^2} \tag{8}$$

$$Rx_{Sensitivity} = \frac{V}{P} \propto \frac{F_{eq}}{\eta P} \propto \frac{A}{\eta} \propto \frac{A}{t} \tag{9}$$

where P is the acoustic pressure, d is the transducer displacement, F_{eq} is the equivalent force and A is the device area. The term η is proportional to the active layer thickness t through the term $(z_n - z_i)$ and K_{eq} is proportional to t^3 through the term EI_{eff}. We multiply the reported transmit sensitivities by the respective piezoelectric thicknesses and after normalizing by the transducers area we obtain a figure of merit (FoM) related to the devices receive sensitivities as shown in Fig. 6.

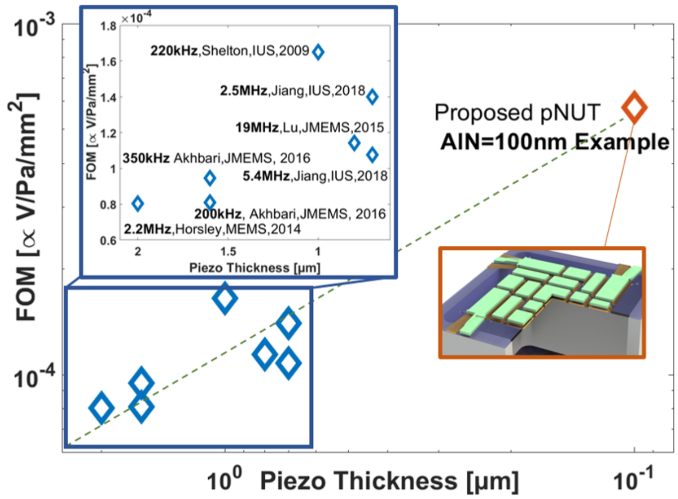

Fig. 6. Comparison of Rx FoM of proposed pNUT and literature data.

A linear trend emerges as the piezoelectric thickness is down-scaled. This suggests that pNUTs are excellent candidates to either dramatically reduce the area of existing devices without losing sensitivity or to be arrayed to boost the receive sensitivity without increasing the total footprint.

REFERENCES

[1] D. E. Dausch, K. H. Gilchrist, J. B. Carlson, S. D. Hall, J. B. Castellucci, and O. T. von Ramm, "In vivo real-time 3-D intracardiac echo using PMUT arrays," *IEEE Transactions on Ultrasonics, Ferroelectrics, and Frequency Control*, vol. 61, pp. 1754–1764, 10 2014.

[2] Y. Lu, H. Tang, S. Fung, Q. Wang, J. M. Tsai, M. Daneman, B. E. Boser, and D. A. Horsley, "Ultrasonic fingerprint sensor using a piezoelectric micromachined ultrasonic transducer array integrated with complementary metal oxide semiconductor electronics," *Applied Physics Letters*, vol. 106, p. 263503, 6 2015.

[3] A. S. Rekhi, B. T. Khuri-Yakub, and A. Arbabian, "Wireless Power Transfer to Millimeter-Sized Nodes Using Airborne Ultrasound," *IEEE Transactions on Ultrasonics, Ferroelectrics, and Frequency Control*, vol. 64, pp. 1526–1541, 10 2017.

[4] X. Jiang, G. Luo, Q. Wang, and D. A. Horsley, "Improving PMUT Transmit Performance via Sub-Micron Thickness Scaling," in *2018 IEEE International Ultrasonics Symposium (IUS)*, pp. 1–9, IEEE, 10 2018.

[5] P. W. Eaton, F. Bitsie, J. H. Smith, and D. W. Plummer, "A New Analytical Solution for Diaphragm Deflection and its Application to a Surface-Micromachined Pressure Sensor," in *TechConnect Briefs*, p. 6, Computational Publications, 4 1999.

[6] M. Weinberg, "Working equations for piezoelectric actuators and sensors," *J. MEMS*, vol. 8, no. 4, pp. 529–533, 1999.

[7] D. Kim, M. L. Kuntzman, and N. Hall, "A transmission-line model of back-cavity dynamics for in-plane pressure-differential microphones," *The Journal of the Acoustical Society of America*, vol. 136, pp. 2544–2553, 11 2014.

[8] G. Massimino, L. D'Alessandro, F. Procopio, R. Ardito, M. Ferrera, and A. Corigliano, "Air-coupled PMUT at 100 kHz with PZT active layer and residual stresses: Multiphysics model and experimental validation," in *2017 18th International Conference on Thermal, Mechanical and Multi-Physics Simulation*, pp. 1–4, IEEE, 4 2017.

[9] B. A. Griffin, M. D. Williams, C. S. Coffman, and M. Sheplak, "Aluminum Nitride Ultrasonic Air-Coupled Actuator," *JOURNAL OF MICROELECTROMECHANICAL SYSTEMS*, vol. 20, no. 2, 2011.

[10] J. Best and G. Piazza, "Electrostatic actuation of the pulse-activated Piezo-NEMS shuttle relay," in *2018 IEEE Micro Electro Mechanical Systems (MEMS)*, pp. 638–641, IEEE, 1 2018.

[11] U. Zaghloul and G. Piazza, "Sub-1-volt Piezoelectric Nanoelectromechanical Relays With Millivolt Switching Capability," *IEEE Electron Device Letters*, vol. 35, pp. 669–671, 6 2014.